CONF-9506256--1

LA-UR-95-2664

Title: SUPRATHERMAL ELECTRON LOSS CONE DISTRIBUTIONS IN THE SOLAR WIND: ULYSSES OBSERVATIONS

Author(s): J. L. Phillips
W. C. Feldman
J. T. Gosling
C. M. Hammond
R. J. Forsyth

Submitted to: Proceedings of the Eighth International Solar Wind Conference
Dana Point, CA
June 26-30, 1995

DISCLAIMER

Portions of this document may be illegible in electronic image products. Images are produced from the best available original document.

Suprathermal Electron Loss Cone Distributions in the Solar Wind: Ulysses Observations

J.L. Phillips, W.C. Feldman, and J.T. Gosling
Los Alamos National Laboratory

C.M. Hammond
SRI International

R.J. Forsyth
Imperial College

Abstract. We present observations by the Ulysses solar wind plasma experiment of a new class of suprathermal electron signatures. At low solar latitudes and heliocentric distances beyond 3.37 AU Ulysses encountered seven intervals, ranging in duration from 1 hour to 22 hours, in which the suprathermal distributions included an antisunward field-aligned beam and a return population with a flux dropout typically spanning ±60° from the sunward field-aligned direction. All events occurred between the forward and reverse shocks or waves bounding corotating interaction regions (CIRs). The observations support a scenario in which the sunward-moving electrons result from reflection of the prevailing antisunward field-aligned beam at magnetic field compressions downstream from the spacecraft, with wide loss cones caused by the relatively weak mirror ratio. This hypothesis requires that the field magnitude within the CIRs actually increased locally with increasing field-aligned distance from the Sun.

Introduction

Solar wind electrons distributions comprise a thermal (or "core") population and a suprathermal (or "halo") distribution. The halo distribution carries an antisunward field-aligned heat flux driven by the temperature difference between the hot corona and cold interplanetary space [e.g., *Feldman*

et al., 1975]. The field-aligned component of the halo is often sharply peaked in angle and is sometimes known as the "strahl" [*Rosenbauer et al.,* 1976]. In closed magnetic regions such as coronal mass ejections, as well as when magnetically connected to a second heat source such as a shock, the electron heat flux is often observed to flow in both directions along the interplanetary magnetic field [e.g., *Bame and Gosling,* 1989; *Gosling et al.*, 1993].

Solar rotation and the tilt of the Sun's magnetic dipole cause fast wind from the polar coronal holes to overtake slower wind from the heliomagnetic streamer belt at low heliographic latitudes. Regions of compressed plasma, called corotating interaction regions (CIRs), develop at the interface between fast and slow wind. Beyond ~2 AU the compression waves bounding CIRs commonly steepen into leading forward shocks and trailing reverse shocks [e.g., *Hundhausen and Gosling*, 1976; *Smith and Wolfe*, 1976].

The Ulysses spacecraft was launched in October 1990, cruised in the ecliptic plane to 5.4 AU for a gravity assist at Jupiter in February 1992, then turned south. Peak southerly latitude of -80° was reached in September 1994; aphelion was at 1.3 AU in March 1995. Data used in this study include suprathermal electron distribution functions and bulk ion parameters from the electron and ion spectrometers of the solar wind plasma experiment [*Bame et al.*, 1992], as well as 256-second averaged magnetic field measurements from the dual magnetometer experiment [*Balogh et al.*, 1992]. Data from the entire mission through May 1995 were surveyed.

An Unusual Event

Color-coded spectrograms of electron counts are routinely used by the Ulysses plasma team as a tool for surveying electron distribution shapes. In some of these displays, electron count rates are plotted versus spin angle for various energy ranges. The antisunward electron strahl typically appears as a single magnetic field-aligned beam that propagates away from the Sun. In CMEs and

other closed structures, as well as in some electron foreshocks, two field-aligned beams are seen centered in opposite directions. The present study focuses on events which have distinctive signatures in the color spectrograms which appear as three stripes: a conventional antisunward strahl in one hemisphere, and two thinner enhancements in the other hemisphere, bracketing a field-aligned dropout.

An example of a single electron spectrum from one of these unusual events is shown in Figure 1. The plot shows electron phase space density versus energy and spacecraft spin angle. The positions of $\pm\mathbf{B}$ are marked at the top; the field vector was inclined only 2° from the spin plane for this spectrum. Labels at right indicate the approximate ranges of core and halo solar wind electrons, plus very low energy photoelectrons emitted from the spacecraft and electrostatically trapped. The shaded box surrounds the region of interest, the lower-energy suprathermal or halo population, in which the unusual distribution shape can be seen. Within this box one can see a spin modulation which includes a field-aligned enhancement along $+\mathbf{B}$, corresponding to antisunward electron motion, plus a return distribution with two enhancements centered on a field-aligned minimum at $-\mathbf{B}$.

Figure 2 shows a closer look at the same electron distribution shown in Figure 1, including counts versus angle displays for three halo energies. The $\pm\mathbf{B}$ directions are marked by vertical traces. At each of the energies shown, one can see a strong enhancement in the $+\mathbf{B}$ direction at +90° spin angle, representing antisunward propagation along the tightly-wound interplanetary spiral, and twin enhancements bracketing the conjugate spin angle (-90°). The non-gyrotropicity (e.g., the higher count rates at +60° than at +120°) was due to solar wind convection and was most pronounced at the lowest energy shown (44 eV). Heavy dots mark the two peaks at 44 eV in the sunward field-centered hemisphere (-180° to 0°). In order to compare the two hemispheres, these dots were also plotted in the antisunward field-centered hemisphere by reflecting them across the 0° position. Note that phase space densities for the sunward peaks nearly match those at

corresponding points in the opposite hemisphere (the heavy dots near 30° and 130° lie very near the 44 eV trace). For all distributions in all the events surveyed, the count rates in the two sunward peaks were similar to or lower than those at corresponding points in the antisunward hemisphere.

Our working hypothesis is that the peaks in the return hemisphere were caused by magnetic mirroring of the antisunward field-aligned strahl. The mirror ratio, B_{mirror} / B_{local}, was relatively weak, resulting in mirroring only of higher pitch-angle particles and creation of a wide loss cone in the sunward-directed hemisphere.

Figure 3 shows the solar wind context of the event featured in Figures 1 and 2, including proton density, temperature, flow speed, and azimuthal flow angle, as well as magnetic field magnitude and radial component. The loss cone interval is marked by a heavy bar. This event occurred within a CIR that was bounded by a leading forward shock and a trailing reverse wave. The locations of these features and of the stream interface [e.g., *Burlaga*, 1974] are marked by vertical dashed traces; the stream interface location was identified primarily by analysis of proton temperature and flow angle. Note that for most of the CIR interval, including the loss cone event, the magnetic field was nearly transverse (i.e., small radial component), and that the event was observed after crossing the stream interface.

Observational Summary and Interpretation

The entire Ulysses plasma electron data set through May 1995 was searched for electron distributions of the type shown in Figures 1 and 2, using color spectrograms and other displays. Seven events were found, one of which was split by an interval of conventional unidirectional heat flux. The event times, solar wind contexts, and loss cone characteristics are shown in Table 1. The observations are summarized as follows: (1) The loss cone intervals ranged from 1 hour to 22 hours in duration. (2) All seven events occurred within CIRs between 3.37 and 5.4 AU

(aphelion), at low heliographic latitudes. All CIRs had leading forward shocks; not all had trailing reverse shocks. (3) Five of the seven events occurred after crossing the CIR stream interface; one was before the interface, and one was unclear. (4) All events occurred during intervals when the magnetic field was largely transverse to the radial direction. (5) For each event, the conventional field-aligned strahl was in the hemisphere appropriate for antisunward propagation, while the double-peaked distribution was in the sunward-propagating hemisphere. (6) For each event, the phase space density of the return peaks was comparable to, or smaller than, phase space density at corresponding points in the antisunward-moving distribution. (7) The loss cone half-widths ranged from 50° to 76°, corresponding to mirror ratios of 1.70 to 1.06, respectively.

The electron spectra presented here are clearly consistent with reflection of the antisunward field-aligned electron strahl by an enhanced magnetic field region located farther from the Sun on the same field line. The large loss cones dictate a relatively weak mirror ratio. The mirror hypothesis requires that, under some circumstances, field magnitude actually increases with increasing distance from the Sun within a CIR. The fact that the events are only seen beyond 3.37 AU is consistent with this argument, for the following reasons: (1) CIR compressions are stronger at 3-5 AU than at smaller heliocentric distances. (2) CIRs tend to take on a Parker-spiral alignment, which becomes increasingly transverse to the radial direction with increasing R. Beyond a few AU from the Sun, the field-aligned path incorporates a relatively small change in R and thus should involve a relatively small decrease in the prevailing |B| with increasing distance along **B**. A locally enhanced compression has to overcome only a small field gradient to produce a mirror geometry. (3) For any field orientation (radial, transverse, or spiral), $|\partial B/\partial R|/|B|$ decreases with increasing heliocentric distance, again making it easier for a local compression to overcome this prevailing gradient.

Electron velocity distributions with twin enhancements bracketing the antisunward strahl were observed by ISEE-3 downstream of some interplanetary shocks at 1 AU [*Feldman et al.*, 1983; see

Figure 3], and were attributed to shock heating. However, those distributions were fundamentally different in that the enhancements were at ±90° from **B**, whereas the Ulysses enhancements were at acute angles from ±**B** in the sunward field-centered hemisphere. While it is difficult to ascertain whether a given interplanetary field line has passed through a shock, we believe that it was field compression, and not shock-related processes, that caused the Ulysses electron signatures. Note that two of the events (the first and fifth events in Table 1) occured within CIRs bounded on the trailing edge by a reverse wave, not a shock. For both of those events the loss cone distributions were observed after the stream interface, indicating that the event field lines had not been shocked.

Our concept of the magnetic mirror geometry is shown schematically in Figure 4. The relative scarcity of the loss-cone events argues that the magnetic mirror configuration is not a prevailing characteristic of CIRs beyond 3 AU, but results from local inhomogeneities in solar wind characteristics and hence in the compression at the CIR. Complete reflection of the antisunward strahl so as to create a bidirectional electron signature, as suggested by *Kahler and Reames* [1991] would of course require an infinite field compression [cf. *Gosling et al.*, 1992]. The minimum loss cone half-angle of 50° observed in the Ulysses data is far larger than the angular resolution of modern plasma spectrometers, suggesting that downstream field compressions strong enough to create return distributions with no observable loss cone are rare or nonexistent.

Acknowledgments. Work at Los Alamos was performed under the auspices of the U.S. Department of Energy with financial support from NASA.

References

Balogh, A., et al., The magnetic field investigation on the Ulysses mission: Instrumentation and preliminary scientific results, *Astron. Astrophys. Supp. Ser. 92*, 221, 1992.

Bame, S. J., and J. T. Gosling, Bidirectional electron heat flux events in space, in *Proceedings of the Second International Workshop on the Relation Between Laboratory and Space Plasmas*, edited by Hiroshi Kikuchi, p. 347, Springer-Verlag, New York, 1989.

Bame, S. J., et al., The Ulysses solar wind plasma experiment, *Astron. Astrophys. Supp. Ser. 92*, 237, 1992.

Burlaga, L. F., Interplanetary stream interfaces, *J. Geophys. Res., 79*, 3717, 1974.

Feldman, W. C., et al., Solar wind electrons, *J. Geophys. Res., 80*, 4181, 1975.

Feldman, W. C., et al., Electron velocity distributions near interplanetary shocks, *J. Geophys. Res., 88*, 9949, 1983.

Gosling, J. T., D. J. McComas, and J. L. Phillips, Counterstreaming Electron Events on Open Field Lines?, in *Solar Wind Seven*, edited by E. Marsch and R. Schwenn, Pergamon Press, Oxford, p. 619, 1992.

Gosling, J. T., et al., Counterstreaming suprathermal electron events upstream of corotating shocks in the solar wind beyond ~2 AU: Ulysses, *Geophys. Res. Lett., 20*, 2335, 1993.

Hundhausen, A. J., and J.T. Gosling, Solar wind structure at large heliocentric distances: An interpretation of Pioneer 10 observations, *J. Geophys. Res., 77*, 5442, 1976.

Kahler, S. W., and D. V. Reames, Probing the Magnetic Topologies of Magnetic Clouds by Means of Solar Energetic Particles, *J. Geophys. Res.., 96*, 9419, 1991.

Rosenbauer, H., et al., Preliminary results of the Helios plasma measurements, in *Physics of Solar Planetary Environments*, edited by D.J. Williams, p. 319, AGU, Washington, D.C., 1976.

Smith, E. J., and J. H. Wolfe, Observations of interaction regions and corotating shocks between one and five AU: Pioneers 10 and 11, *Geophys. Res. Lett., 3*, 137, 1976.

Table 1. Summary of loss cone events.

Event Start (UT)	End (UT)	R(AU)	Helio-latitude	Forward shock	Reverse Shock (Wave*)	Stream Interface	Loss Cone Half-Angle	Mirror Ratio
0945 18JUN91	1100 18JUN	3.37	-4.9°	2300 17JUN	1710 19JUN*	0800 18JUN	50°-60°	1.33-1.70
2030 06JUL91	0045 07JUL	3.54	-5.0°	0218 04JUL	1634 07JUL	1330 05JUL	56°-60°	1.33-1.45
0950 02AUG91	1200 02AUG	3.80	-5.2°	0334 01AUG	1322 04AUG	1800 01AUG	60°-64°	1.24-1.33
1930 02AUG91	1730 03AUG						60°-68°	1.16-1.33
1230 21SEP91	1800 21SEP	4.24	-5.5°	1522 20SEP	1536 23SEP	2000 21SEP	52°-60°	1.33-1.61
0140 21OCT91	0715 21OCT	4.50	-5.6°	0440 19OCT	1245 22OCT*	0400 20OCT	52°-60°	1.33-1.61
1700 10MAR92	2400 10MAR	5.40	-7.6°	0300 09MAR	NONE	UNCLEAR	50°-56°	1.45-1.70
0915 23JUL92	1015 23JUL	5.32	-14.3°	0545 20JUL	1852 23JUL	1600 22JUL	72°-76°	1.06-1.11

Figure Captions

Fig. 1. Electron spectrum, plotted as phase space density versus spin angle and energy. Shaded box shows region of interest.

Fig. 2. Counts versus spin angle for three suprathermal energies, for the same spectrum shown in Figure 1. Heavy dots at -130° and -30° mark peaks of return distribution at 44 eV; dots at +30° and +130° mark corresponding points in the antisunward field-centered hemisphere.

Fig. 3. Solar wind context for the event including the spectrum shown in Figures 1 and 2, including proton density, temperature, flow speed, azimuthal flow angle, and magnitude and radial component of the magnetic field from 1200 UT on 17 June 1991 through 2400 UT on 19 June 1991. Vertical dashed traces mark the leading forward shock, stream interface, and trailing reverse wave of the CIR; heavy bar marks the loss cone event.

Fig. 4. Cartoon illustrating the postulated field geometry for a weak magnetic mirror within a CIR.

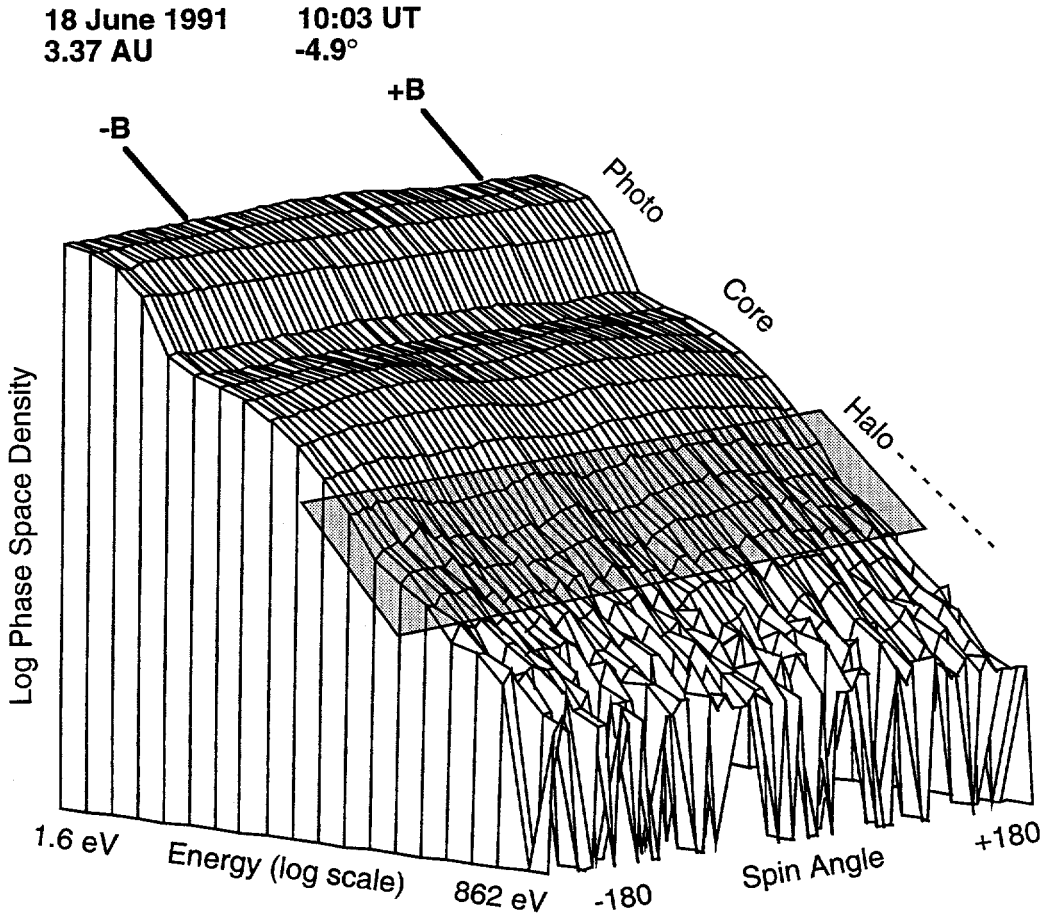
18 June 1991
3.37 AU
10:03 UT
-4.9°
+B
-B
Photo
Core
Halo
Log Phase Space Density
1.6 eV
Energy (log scale)
862 eV
-180
Spin Angle
+180

FIG. 1

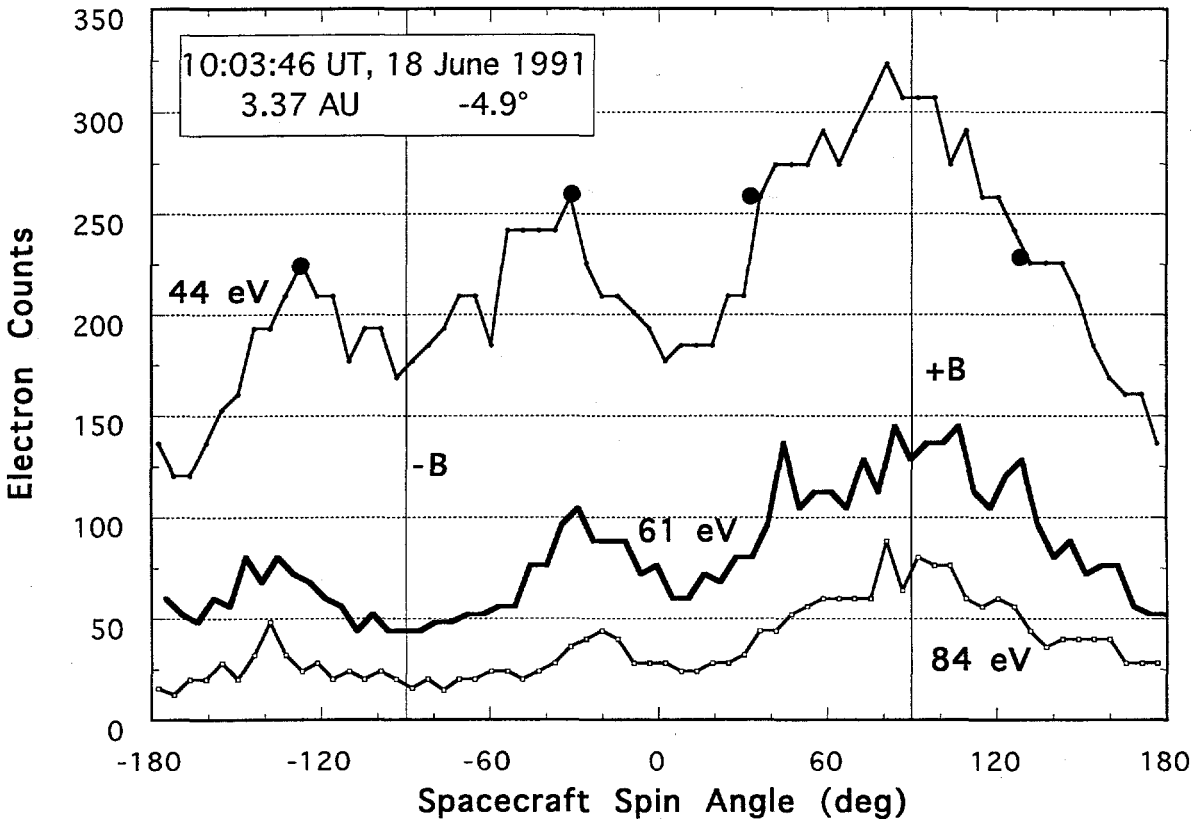
10:03:46 UT, 18 June 1991
3.37 AU -4.9°
44 eV
61 eV
84 eV
-B
+B
Electron Counts
Spacecraft Spin Angle (deg)
350
300
250
200
150
100
50
0
-180
-120
-60
0
60
120
180

FIG. 2

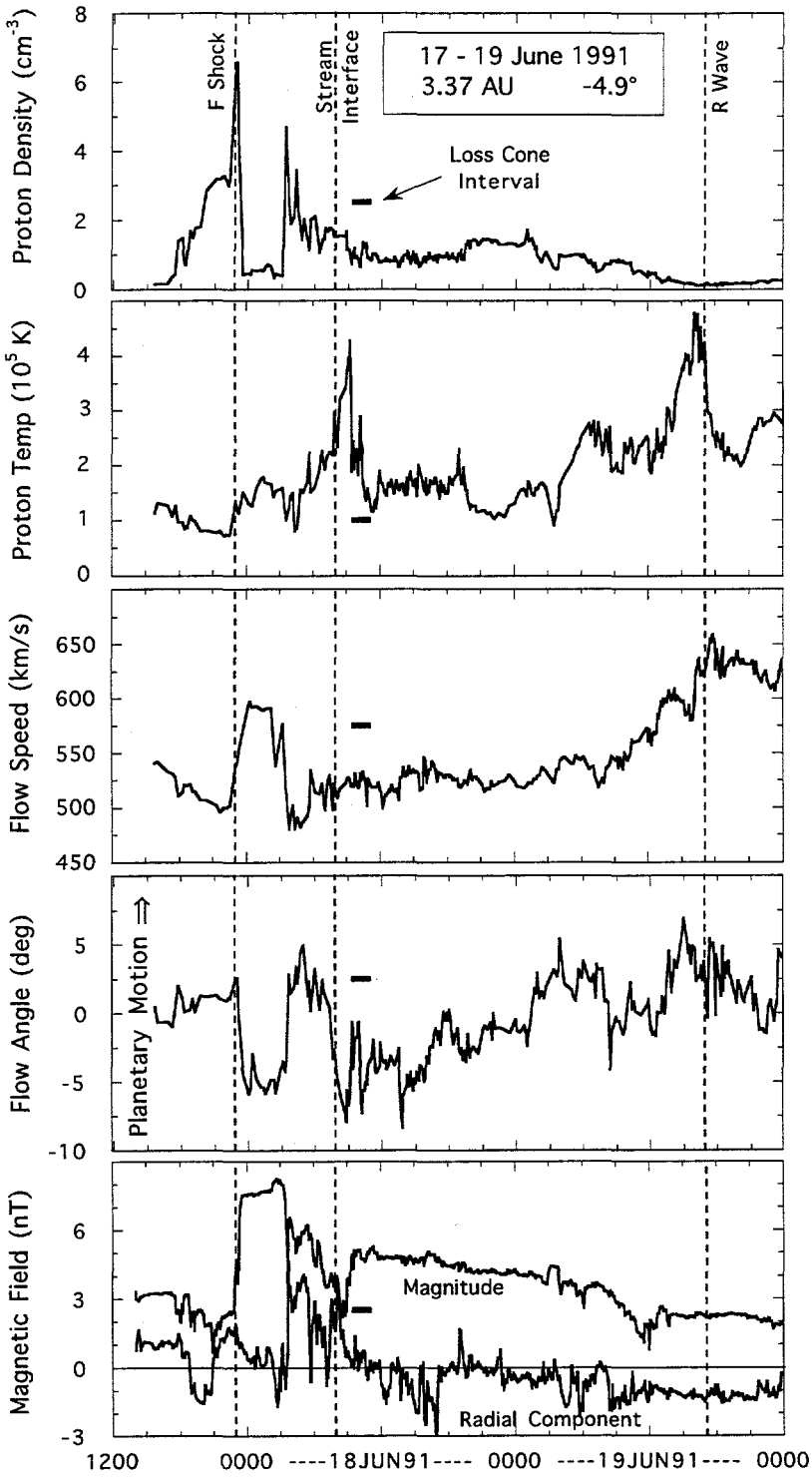
Proton Density (cm^{-3})
F Shock
Stream Interface
17 - 19 June 1991
3.37 AU -4.9°
R Wave
Loss Cone Interval
Proton Temp (10^5 K)
Flow Speed (km/s)
Flow Angle (deg)
Planetary Motion ⇑
Magnetic Field (nT)
Magnitude
Radial Component
1200 0000 ----18JUN91---- 0000 ----19JUN91---- 0000

FIG. 3

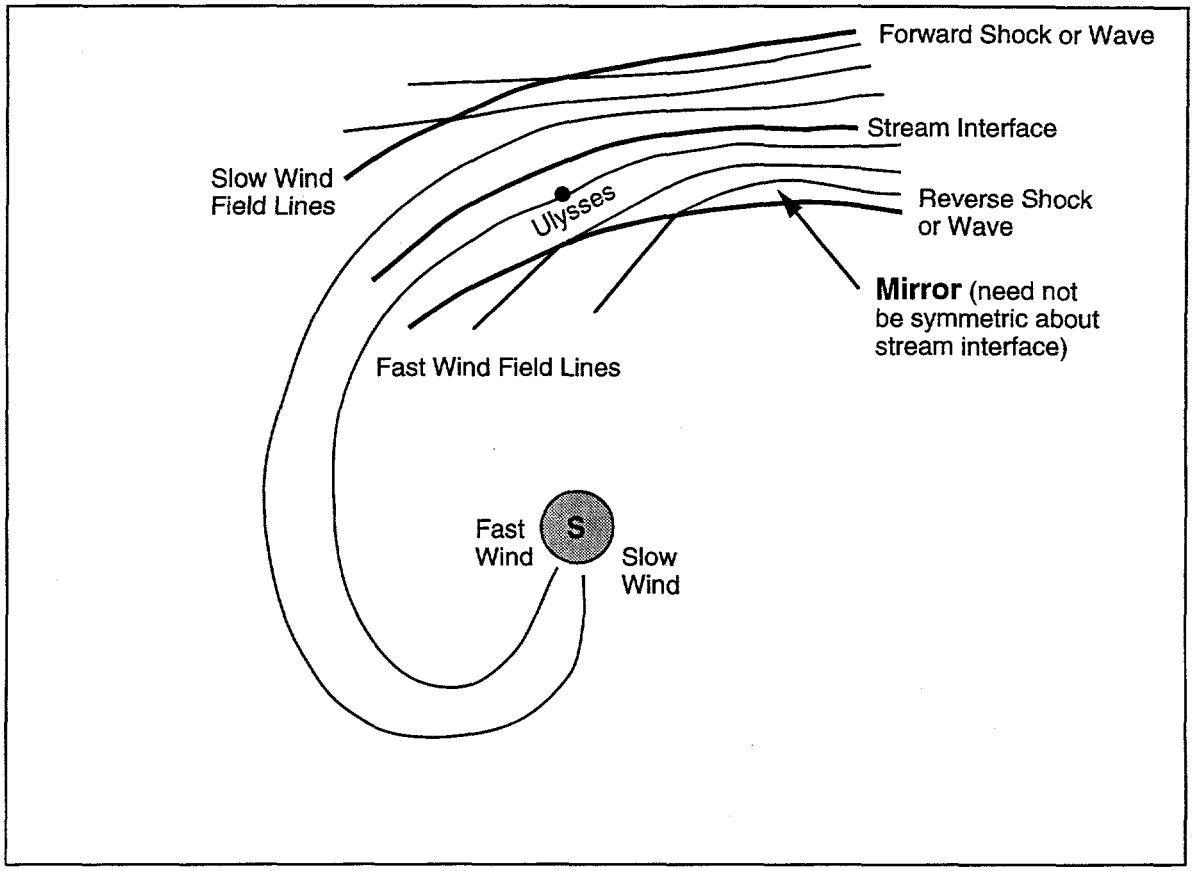
Forward Shock or Wave
Stream Interface
Slow Wind
Field Lines
Ulysses
Reverse Shock
or Wave
Mirror (need not
be symmetric about
stream interface)
Fast Wind Field Lines
Fast
Wind
S
Slow
Wind

FIG. 4